

# Salinity Variations in the Southern California Current

**Niklas Schneider**

International Pacific Research Center and Department of Oceanography, University of Hawaii at Manoa, Honolulu, Hawaii

**Emanuele Di Lorenzo**

School of Earth and Atmospheric Sciences, Georgia Institute of Technology, Atlanta, Georgia

**Peter P. Niiler**

Scripps Institution of Oceanography, University of California, San Diego, La Jolla, California

Corresponding author:

N. Schneider, IPRC, University of Hawaii at Manoa, 1680 East West Road, Honolulu, HI 96822. Phone (808) 956-8383, fax (808) 956-9425, email: nschneid@hawaii.edu

**Abstract.** Hydrographic observations south-westward of the Southern California Bight in the period 1937-2003 show that temperature and salinity variations have very different interannual variability. Temperature varies within and above the thermocline and is correlated with climate indices of El Niño, the Pacific Decadal Oscillation, and with local upwelling. Salinity variability is largest in the surface layers of the offshore salinity minimum, and is characterized by decadal time-scale changes. The salinity anomalies are independent of temperature, of heave of the pycnocline, and of the climate indices. Our calculations demonstrate that long-shore anomalous geostrophic advection of the mean salinity gradient accumulates along the mean southward trajectory along the California Current, and produces the observed salinity variations. The flow anomalies for this advective process are independent of large scale climate indices. We hypothesize that low frequency variability of the California Current System results from unresolved, small-scale atmospheric forcing or from the ocean mesoscale upstream of the Southern California Bight.

## 1. Introduction

The California Current transports cool, fresh and nutrient-rich waters from the North Pacific equatorward, and together with coastal upwelling, supports a highly productive and complex ecosystem. This system has sparked the interest of oceanographers since the early part of the 20th century, and today more than 63 years of ocean observations provide an unique opportunity to investigate multi-year and decadal changes in this eastern boundary current. Here, pronounced interannual to decadal variability of salinity in the California Current off Southern California is investigated.

The California Current System varies on multiple time scales, and reflects mesoscale processes, seasonal forcing, and remote forcing. Variability of sea surface temperature (SST) and sea level has been documented in a number of studies, and consistent relationships with local and remote forcing have been established. Changes of salinity, however, have received only intermittent attention, and no clear description of its anomalies has emerged.

Interannual anomalies of SST and sea level along the Pacific coast of North America are linked to equatorial and North Pacific wind stress, with the tropical influence dominant south of 31°N (Chelton and Davis 1982, Lluch-Cota et al. 2001). During El Niño, sea level along the coast of California rises (Chelton and Davis 1982), the thermocline deepens, and SST increases by typically 1.5°C, particularly during winter (McGowan et al. 1998, Lluch-Cota et al. 2001). During La Niña the response is reverse but weaker, and SST anomalies are typically cooler by 1°C (McGowan et al. 1998).

El Niño induces SST anomalies along the coast of California after a lag of zero to two seasons with no discernible phase propagation from the tropics. Regional atmospheric forcing generates temperature and sea level anomalies in the Northeast Pacific (Emery and Hamilton 1985), and, during the 1997-98 El Niño, in the California current (Schwing et al. 2002).

SST variability in the California current is also coherent with anomalies in the central North Pacific at interannual and longer time scales. The leading empirical orthogonal function (EOF) of SST in the North Pacific, the Pacific Decadal Oscillation (PDO, Davis 1976, Mantua et al. 1997, Schneider and Cornuelle 2004), has strong loading along the coast of California, with signs opposite to the central North Pacific. The 'climate shift' of 1976/77 (Trenberth 1990) warmed the California Current (Bograd and Lynn 2003) through altered air-sea heat fluxes and Ekman advection (Miller et al. 1994). The warming continued through the 1990s (Roemmich 1992) in concert with a depression of the main thermocline and a marked decrease of zooplankton (Roemmich and McGowan 1995). Since local, upwelling favorable winds had increased (Bakun 1990, Schwing and Mendelson 1997), the warming and changes in thermocline depth resulted either from equatorial wind stress anomalies and wave propagation along the western coast of America (Clarke and Lebedev 1999), or from surface heat flux anomalies (Di Lorenzo et al. 2004) and a local wind stress curl that affected temperatures above the top of the thermocline and reduced the horizontal slope of the thermocline (Roemmich and McGowan 1995).

Salinity in the California Current varies on decadal and interannual time scales.

After the 1976/77 shift, surface salinity within 500 km of the coast decreased by less than 0.1 psu, and subsurface salinity offshore increased by up to 0.1 psu (Bograd and Lynn 2003). Decadal changes of salinity include a decrease of 0.2 psu from 1981 to 1994 off southern California (Roemmich and McGowen 1995), and a salinity increase by up to 0.15 psu at the 10°C isotherm due to a lateral shift of water masses associated with a downward displacement of isotherms. Along central and northern California coastal stations, increases of upwelling inducing winds (Bakun 1990) during the last decades increased salinities along the coast (Schwing and Mendelsohn 1997). It is not clear from previous studies whether the increase of salinity at the 10°C isotherm come from salty water along the coast or lateral movement from off shore.

Various relationships of ENSO and salinity in the California Current system have been reported. Conclusions drawn from data before 1984 are that during El Niño a freshening of the upper layers occurs (Hickey 1998). However, more recent observations indicate that results differ between episodes. The 1941-1942, 1982-83 and 1991-92 El Niños were associated with fresh offshore anomalies (Simpson 1992, Ramp et al. 1997), while during the 1997/1998 El Niño surface waters off southern California were saltier compared to La Niña events of 1996 and 1999 (Lynn and Bograd 2002).

Decadal salinity anomalies in the California Current have been used to delineate the effects of upwelling and long-shore advection on the nutrient budget and biological productivity (Chelton 1981, Chelton et al. 1982). Upwelling and equatorward advection both supply nutrients to the surface layer, but upwelling brings saltier waters from the halocline to the surface while equatorward advection freshens the surface layer. Since

high zooplankton concentrations are associated with low salinity and southward flow anomalies, lateral advection is the likely source of nutrient anomalies in the off-shore, central part of the California Current.

The purpose of this study is to investigate interannual and decadal variations of upper ocean salinity in the California Current system southwest of the Southern California Bight, using observations over a 63 years time span. We use hydrographic data along a line southwest from the Bight that has more observations than any other segment of the California Current. In section 2, the data and their analysis are discussed, followed by a comparison of temperature and salinity variations. Next, the relationships with local and large scale indices of Pacific climate variability are presented. We then show that long-shore advection by anomalies of the California Current is the most likely mechanism consistent with the observations, and close with conclusions and implications.

## **2. Data**

### **2.1. Hydrography**

The principal data are temperature and salinity observations along a section from Long Beach, CA to  $124^{\circ}\text{W}$ ,  $30^{\circ}30'\text{N}$ , more than 600 km offshore (Fig. 1), from 1937 to 1999. This section is also line-90 of the California Cooperative Oceanic Fisheries Investigation (CalCoFI) survey that has been sampled from 1949 to present (Bograd and Lynn 2003). Additional observations were collected during the late 1930s by H.

Sverdrup and in several intervening years by the U.S. Coast Guard. The data typically has seasonal or higher time resolution, but with gaps in the late 1940s, between 1976 and 1981, and few observations in the offshore regions from 1953 to 1958 (Fig. 2). The station pattern has changed over time, and has samples every 30 to 60 km, with the finer spacing close to the coast (Fig. 3). The CalCoFI data base can be obtained from <http://www.calcofi.org/data/data.html>.

Observations of temperature and salinity are provided at eleven standard depths in the top 500 m of the water column, from which density and potential density are calculated. At every vertical level, the data are then optimally interpolated to a regular spatial grid and three month averages using a Gaussian covariance function with widths of 100 km in the horizontal and 150 days in time, and a signal-to-noise ratio of 0.1. Interpolated points removed by more than 2 Gaussian widths from the closest observation are marked as missing. Note that this interpolation smoothes the data compared to analyses that retain the variable station spacing (Bograd and Lynn 2003). The climatological seasonal cycle is obtained by a least square fit of annual and semi-annual harmonics, and anomalies are estimated as deviations thereof.

Pressure and geostrophic velocities across line-90 are calculated relative to 500 m. In the following, we will use estimates of the anomalous, long-shore geostrophic flow in the center of the section from  $122.5^{\circ}\text{W}$  to  $120^{\circ}\text{W}$ . To achieve a robust estimate that takes advantage of as much of the data as possible, the geostrophic flow anomalies are estimated from the regression of the pressure field to pressure indices averaged inshore and offshore of  $121.5^{\circ}\text{W}$  and in the top 50 m of the water column.

## 2.2. Climate indices

Conditions in the eastern North Pacific are characterized by climate indices of the El Niño–Southern Oscillation (ENSO), the Pacific Decadal Oscillation (PDO), and along-shore wind that produces upwelling along the west coast of North America. Three month averages of all indices are formed to match the time resolution of the ocean observations with the center month shifted to explore correlations with monthly lags.

ENSO is measured by the average sea surface temperature in NINO3.4, an area in the eastern equatorial Pacific ( $170^{\circ}\text{W}$ - $120^{\circ}\text{W}$ ,  $5^{\circ}\text{S}$ - $5^{\circ}\text{N}$ ). Its time series is provided by the National Environmental Prediction Center of the National Oceanic and Atmospheric Administration, and was obtained from <http://www.cdc.ncep.noaa.gov/data/indices/index.html>.

The PDO indices are based on the leading empirical orthogonal function (EOF) of SST in the Pacific north of  $30^{\circ}\text{N}$  (PDO/SST: Mantua et al. 1997, Zhang et al. 1997), and on the North Pacific sea level pressure averaged from  $30^{\circ}$  to  $65^{\circ}\text{N}$  and  $160^{\circ}\text{E}$  to  $140^{\circ}\text{W}$  (PDO/AP: Trenberth and Hurrell 1994). For interannual time scales, these two indices are highly correlated, and will be reported together. PDO/SST is available from <http://jisao.washington.edu/pdo/PDO.latest>, and PDO/AP was obtained from <http://www.cgd.ucar.edu/~jhurrell/np.html>.

Upwelling in the California Current region is characterized by the long-shore component of the wind stress, with positive values of the index corresponding to increased upwelling. This index (CCUP) is calculated from the NCEP/NCAR reanalysis

(Kalnay et al. 1996) as the average, long-shore wind stress from 33°N to 38°N within 300 km of the coast of California (the first grid point fully in the ocean). A trend to stronger winds (Schwing and Mendelsohn 1997) is removed, to avoid spurious correlations in the subsequent analysis. CCUP and the curl of the wind stress on line 90 are correlated at 0.7, and CCUP is therefore an index for coastal and offshore upwelling.

### 3. Climatology of CalCoFI Line-90

#### 3.1. Large-scale context

Line-90 crosses the Southern California Bight and continues through the equatorward flowing California Current to the offshore waters of the eastern Pacific (Fig. 1). The region around line-90 experiences a net upwelling of cool and salty water at a rate of  $3.4 \times 10^{-4} \text{ cm s}^{-1}$ , with large variability, a net mean heat gain of 70-90  $\text{W m}^{-2}$ , and a net loss of fresh water through evaporation of more than  $100 \text{ cm yr}^{-1}$  (Roemmich 1989, Bograd et al. 2001).

The core of the California Current transports low salinity subarctic waters into the higher salinity subtropics. Because the rate of southward transport, and the rate of coastal upwelling of higher salinity are larger than the rate of horizontal mixing by ocean mesoscale eddies (Swenson and Niiler 1996, Cornuelle et al. 2000) or cross isopycnal diffusion, a surface salinity minimum is located several hundred kilometers off-shore (Fig. 1, left). The southward advective convergence of salinity in a distribution of mean salinity in Fig. 1 by a current of 4 cm/sec (Miller et al. 1999) distributed over

50 m of the upper layer is about 20 times larger than the surface flux of salt caused by evaporation of 100 cm/year. Thus, we anticipate that changes in evaporation are not as effective in producing surface salinity anomalies as are changes in southward advection. Because there is a significant equatorward gradient of salinity, an increase of the strength of the southward flow would result in a decrease of salinity at line-90. Because there is an increase of salinity toward the coast, increased off-shore flow would result in an increase of salinity simply due to the changes in the advection of the mean distribution of salinity.

SST decreases toward the north, and, north of Point Conception, decreases toward the coast (Fig. 1, center). The SST distribution is produced by the combined effects of net heating by the atmosphere, equatorward advection, coastal upwelling and horizontal mixing by ocean mesoscale and cross isopycnal diffusion (Marchiesiello et al. 2003).

Density (Fig. 1, right) varies little in the long-shore direction, since the density tendencies of poleward decreasing temperature and salinity balance. The cross-shore density gradients, in contrast, are substantial in-shore of the salinity minimum, since temperature and salinity both contribute to an increase the density toward the upwelling regions. Offshore of the salinity minimum, salinity and temperature increase and balance in their contribution to density, leading to small density gradients.

### **3.2. Temperature, salinity and velocity sections**

In the context of the large scale structure of the California Current system, line-90 crosses through the coastal northward flowing currents, the Point Conception upwelling

plume and the off-shore branch of the California Current. The thermocline (Fig. 4, top) is located between 100–200m, with an upward bulge at 119°W that marks the center of the cyclonic circulation relative to 500 m around the Southern California Bight. The thermocline also coincides with a halocline that varies in depth between 170 m offshore, and 120 m close to the coast, with low salinity waters at the surface and a salinity minimum centered between 123° and 120°W (Fig. 4, center). The 500 m relative geostrophic velocity normal to line-90 (Fig. 4, bottom) is northward in the southern California Bight with a maximum speed at the surface of  $3.0 \text{ cm s}^{-1}$ . Offshore of 119°W, flow is equatorward with multiple cores. Centered at 120°W is a strong jet with a maximum equatorward speed of  $4.9 \text{ cm s}^{-1}$  and further offshore are secondary, weaker jets with maxima of  $2.4$  and  $2.9 \text{ cm s}^{-1}$ . The salinity minimum is associated with the offshore jets because the stronger southward flow core closer to shore contains saltier waters from the Southern California Eddy as well as from the upwelling plume at Point Conception (Di Lorenzo et al. 2004).

These results are qualitatively consistent with Bograd et al. (2001) description of a section approximately 50 km further south using observations from 1984-1997. Bogard et al.'s upper ocean temperatures are approximately  $1^\circ\text{C}$  higher than in the 63 year average shown in Fig. 4, and the maximum normal velocity components were  $9 \text{ cm s}^{-1}$  at the  $12^\circ\text{W}$  core, and  $6 \text{ cm s}^{-1}$  in the offshore region. This reflects the warming of the California Current since 1977 (Roemmich and McGowan 1995), and is consistent with the observed acceleration of the California Current by  $3\text{-}4 \text{ cm s}^{-1}$  in the period 1980-1990 relative to earlier decades (Di Lorenzo et al. 2004).

## 4. Interannual and decadal variability

The time series of the anomalies of line-90 salinity and temperature have different characteristics where salinity variance is dominated by decadal time scales and temperature by interannual time scales and a warming in the two decades after 1977. Since there are many studies of the seasonal cycle in the literature (e.g. Lynn and Simpson 1987, Bray et al. 1999, Di Lorenzo 2003), we focus on the salient features of the interannual and longer term variations.

### 4.1. Salinity and temperature variations and correlations with climate indices

The leading empirical orthogonal function (EOF) of salinity (Fig. 5) captures the essential part of its decadal variability. Its center of action is between  $122^{\circ}$  and  $120^{\circ}$ W in the region of the salinity minimum above the halocline (compare to Fig. 4, center). A secondary maximum is located west of  $123^{\circ}$ W at a depth of 100 to 150m, and coincides with the strong lateral gradient region south-west of the time-mean salinity minimum. Salinity varies by 0.2 psu and was low in the early 1950s, from 1966 to 1971, in 1978 and in the early 1990s. Salinity was anomalous high in the late 1930s, from 1956 to 1965, in the mid 1970s, and around 1990. The decadal variability dominates the variance, and is obvious in the raw observations of surface salinity (Fig. 3).

The leading empirical orthogonal function of temperature (Fig. 6) shows decadal anomalies with cool conditions in the mid 1950s and early 1970s, and warm conditions around 1960 and a pronounced 'shift' in 1976/77 that is followed by a sustained

warming. In addition, the principal component shows interannual variability, with, as shall be discussed more extensively below, warm conditions during the El Niño episodes of the tropical Pacific. Cool conditions have a less reliable relationship with La Niña.

The temperature variability is concentrated above 200 m, with largest values in the upper thermocline and the mixed layer. The loading pattern of the gravest EOF of both salinity and temperature are of single sign, and the principal component time series are therefore nearly identical to the time series of the spatial averages of temperature and salinity anomalies as, for example, reported from these data between 1949 and 1993 by Roemmich and McGowan (1995).

The spectra of the leading principal components of salinity and temperature (Fig. 7) differ in shape at low frequencies. The temperature spectrum shows a peak at interannual time scales and is approximately constant for frequencies smaller than 0.2 cyc a<sup>-1</sup>. The power of salinity increases roughly proportional to frequencies to the power of '-2', and is largest for lowest resolved frequencies, as is apparent in the time series. Interpreted as an autoregressive process driven by white noise (Hasselmann 1976), the damping time scale for salinity corresponds to the lowest resolved frequencies, 0.1 cyc a<sup>-1</sup>, and is 19 months or longer, suggesting that the negative feedbacks on salinity variability are weak.

A significant fraction of the temperature variance is coherent with both ENSO and the PDO time series (Fig. 8, left panel). The lagged correlation of the leading principal component of temperature with NINO3.4 peaks at 0.47 with NINO3.4 leading by one to 5 months. The PDO/SST, has the highest correlation of 0.56 at zero lag, as expected

from the construction of the PDO/SST index. The correlation with the CCUP peaks at modest levels of 0.37, with increased upwelling being associated with cooler conditions.

Through the span of 63 years the leading EOF of salinity at line-90 lacks significant correlations with ENSO, the PDO indices, and CCUP (Fig. 8, right panel). As we will see in the next section, ENSO has a strong correlation with halocline (or thermocline) heave. However, this variance does not project onto the leading mode of salinity variability.

## 4.2. Halocline heave

The time-mean temperature, salinity and density fields imply that long-shore advection displaces thermohaline gradients without causing a density anomalies or dynamical feedbacks. Vertical processes, however, move temperature and salinity stratifications that contribute to density changes in the same way and produce strong dynamical feedbacks to the circulation. This difference, a corollary to the aforementioned function of salinity in determining the roles of long-shore advection and upwelling of nutrients, is used to separate salinity anomalies in the surface layer from changes of the depth of the halocline.

Salinity anomalies  $S'$  are split into parts  $S'_\rho$  and  $S'_\chi$  associated with anomalies of the density  $\rho'$  and independent of density, by considering the in-situ salinity  $S$  and density  $\bar{\rho} + \rho'$  relative to the mean salinity-density relation  $\bar{S}(\rho)$

$$S'_\rho = \bar{S}(\bar{\rho} + \rho') - \bar{S}(\bar{\rho})$$

$$S'_\chi = S - \overline{S}(\overline{\rho} + \rho')$$

where the overbar denotes climatological averages of each season and at each location, and are determined from the data (Church et al. 1991, Bindoff and McDougall 1994). Salinity anomalies  $S'_\rho$  result from a perturbation of the density field, and are determined as the difference of the mean salinity at the in-situ density, and the mean salinity (at the mean density) at this location. Salinity anomalies  $S'_\chi$  on density surfaces are determined as the difference between the in-situ salinity, and the mean salinity at the in-situ density.

The variance of total salinity (Fig. 9) is located at and above the halocline (Fig. 4, center). As expected from the leading EOF, salinity anomalies reach up to 0.15 psu between 122°W and 121°W in the surface salinity minimum, and even larger values at the offshore flank of the minimum. The variance above the halocline is dominated by  $S'_\chi$  (Fig. 9, bottom) and indicate that the salinity variations there are not associated with density variations. Salinity anomalies  $S'_\rho$  dominate in the halocline, and have a weak, but detectable surface maximum on the inshore flank of the salinity minimum at 120°W.

This weakness of  $S'_\rho$  above the halocline occurs despite large variability of density in the upper ocean. A similar split of temperature shows that its variance is dominated by changes of the order of 1°K associated with density and occupy the upper ocean in and above the thermocline. Temperature variations independent of density are also largest in the upper ocean, but only reach values of .5°K.

The time series of  $S'_\rho$  in the halocline at the inshore and offshore centers of action

(Fig. 10) are independent of the leading principal component of salinity. The coastal area has more pronounced interannual variability, while the offshore region is dominated by decadal variability and trend. The coastal signal of  $S'_\rho$  corresponds to a deepened halocline during all El Niño events with the exception of 1954 and 1966 (Fig. 10). The coupling to La Niña events is less tight, in that there are a number of cold events with normal or deepened haloclines, for example 1955, 1968, 1976 and 1985. There are also a number of large anomalies of the halocline not associated with recognized anomalies in the tropical Pacific, such as 1949, 1956, 1957, 1975 and 1994. Nevertheless,  $S'_\rho$  has a high negative correlation with ENSO (Table 1) with a deeper (shallower) halocline and lower (higher) salinities during El Niño (La Niña).

The offshore variability of  $S'_\rho$  has much reduced correlation with ENSO (Table 1), and is dominated by lower frequency variations that indicate a shallow halocline in the mid 1950s and early 1970s, and deep halocline during the early 1950, 1960s through early 1970s, and since the 1980s. Correlations of  $S'_\rho$  with *PDO* are weaker than for the leading principal component of temperature, and suggests that the *PDO* signature in the California Current is partially a result of diabatic changes of the surface layer (Di Lorenzo et al. 2004), rather than vertical deflection of the thermo- and haloclines. The upwelling index has a weak relation with the depth of the halocline, with a sign consistent with increased upwelling leading to a shallower halocline and saltier conditions. Overall, we note, that the variations of the halocline are similar to the leading variations of temperature, and are independent of the leading EOF of salinity.

### 4.3. Implications for vertical and cross-shore transport anomalies

The above analysis shows that the leading EOF of salinity is independent of density variability. This excludes vertical mixing or upwelling as forcing, since these processes act on the strong mean salinity and density gradients and result in correlated anomalies of salinity and density.

Similarly, anomalies of lateral exchanges between the salty and cool upwelling waters and the warmer salinity minimum should leave a signature in density. Anomalies  $S'_\rho$  have weak variability on the inshore flank of the salinity minimum in the upper 50 m of the water column, but are uncorrelated to the main salinity signal, and only of the order of 0.02 psu, much smaller than the offshore variation of salinity. In addition, changes in the eddy or mean transports act on a mean cross-shore difference of salinity (Fig. 4) smaller than 0.2 psu, too small to account for the magnitude, and should produce salinity anomalies that are of opposite signs in and off-shore, unlike the main salinity signal. Thus, local cross-shore exchanges can not be the generation mechanism for the salinity anomalies.

## 5. Salinity anomaly balance

In the following, we will demonstrate that the interannual and decadal salinity variations result from the accumulation of anomalous advection along the mean equatorward trajectory of water in the California Current. The anomalous salinity budget, averaged in cross shore and vertical directions over the core of the salinity signal

close to the surface,

$$\partial_t S' + \langle \bar{v} \partial_y S' \rangle = - \langle v' \partial_y \bar{S} \rangle \quad (1)$$

balances rate of change (storage) of salinity anomalies  $S'$ , advection of  $S'$  by the mean, long-shore current  $\bar{v}$ , and advection by the long-shore current anomalies  $v'$  of the gradient of mean salinity  $\partial_y \bar{S}$ . The brackets  $\langle \dots \rangle$  denote the cross-shore and vertical average over the salinity minimum, i.e. 122.5° to 120°W, surface to 50 m depth.

### 5.1. Rate of change following the mean flow

Salinity variations in the upper ocean do not affect the air-sea fluxes of fresh water (at least for the order of oceanic salinity anomalies) and, compared to variations of the ocean's temperature in the mid- and low latitudes, affect the ocean density and dynamics modestly only. Therefore no process efficiently damps salinity anomalies in the same way as the air-sea heat flux counteracts anomalies of surface temperature. Imbalances in the salt budget lead to a rate of change of salinity, and large variance at low frequencies (Hall and Manabe 1997) as seen in the spectrum of the leading principal components of salinity (Fig. 7). This suggests that storage of salinity is an important process even at interannual and longer time scales.

Since a water particle advected by the California Current with a speed of  $4 \text{ cm s}^{-1}$  travels almost 1300 km in a year, the salinity balance at long time-scales is not local, and the mean long-shore advection has to be considered. Salinity anomalies at line 90 result from the accumulation of the right hand side terms of equation (1) along the mean equatorward trajectory of water in the California Current.

## 5.2. Anomalous advection

Anomalous long-shore advection has been invoked previously to explain the low frequency salinity variations (Chelton et al. 1982). Following this hypothesis, a decrease (increase) of salinity is associated with equatorward (poleward) flow anomalies, where the regression between the rate of change of salinity and the current is the average, long-shore salinity gradient. This hypothesis is tested in two related ways: By comparison of epoch averages of  $\partial_t S'$  and of long-shore geostrophic flow  $v'$ , and by integrating equation (1) and comparing the anomalous along-shore displacement  $\int dt v'$  with salinity.

To determine the rate of change of salinity, we focus on the large salinity signal between  $122.5^\circ$  and  $120^\circ\text{W}$ , in the upper 50 m of the water column. Its time series is virtually identical to the leading EOF of salinity in the entire section. From the time series, epochs are defined based on periods of consistent rate of change of salinity in the salinity minimum (Fig. 11, top), and epoch averaged salinity tendencies are estimated by the least square slope.

The epoch averages (Fig. 11) show decreasing salinities and equatorward current anomalies in epochs centered in years 1951, 1966, and 1987, and increases of salinity and poleward current anomalies in the epochs of 1956 and 1973. This supports the anomalous advection hypothesis. During the late 1990 (epoch centered on 1997) the hypothesis does not work: the flow is equatorward, yet salinities do not decrease.

The scatter plot of epoch averaged salinity tendency and geostrophic flow (Fig.

12) shows the dependence of salinity storage and geostrophic flow, and implies a climatological along-shore salinity gradient of approximately 0.2-0.3psu/1000km, weaker than the climatological salinity field (Fig. 1). Thus, anomalous advection can easily generate the observed salinity anomalies by displacement of the climatological gradients. In fact, the smaller than observed, implied climatological long-shore salinity gradient is consistent with lateral mixing that dilutes and spreads through the entire section the anomalies generated in the California Current.

A more quantitative comparison without the need to subjectively determine epochs is to estimate salinity anomalies from equation (1) forced by anomalous advection. The solution for salinity is then given by the integral of anomalous advection along the particle trajectory from the North Pacific to line-90,

$$S'(y, t) = -\gamma \int_{t - \frac{y - y_0}{\bar{v}}}^t dt' \left[ v' \overline{\partial_y S} \right]_{y - \bar{v}(t - t'), t'} + S'(y_0, t - \frac{y - y_0}{\bar{v}}) \quad (2)$$

where  $y_0$  is the location of upstream condition.

The factor  $\gamma$  describes the dilution due to cross-shore exchanges or due to the operator  $\langle \dots \rangle$  in equation (1) that spreads anomalies generated in the salinity minimum by long-shore advection to salinity anomalies coherent from the coast to the offshore limit of line 90. Thus  $1 \geq \gamma > 0$  where the top range indicates little dilution of the forced anomalies.

This solution shows that upstream boundary conditions and mean advection arrest the growth of variance at low frequencies by limiting the time particles are exposed to anomalous forcing on their transit from upstream locations  $y_0$  with no (or statistically

independent) anomalies.

To solve this equation, upstream salinity has to be specified. The low salinity waters in the California current originate from the North Pacific, about 1500 km up the coast (Fig. 1), and we will assume, for lack of better knowledge, constant salinity there.

Assuming that  $v'\overline{\partial_y S}$  is independent of  $y$ , that is that the anomalous flow is coherent along the California Current (Chelton 1981, Chelton et al. 1982), the solution forced by the observed geostrophic anomalies (Fig. 13, bottom) is shown in Fig. 13 by the dark gray line. To achieve this solution, the integral was evaluated up to four years into the past,  $\gamma = 1/3$ , and an along-shore gradient of salinity (0.5 psu/1000km) was assumed. While the fit is far from perfect, and fails in the second half of the 1960s, the solution captures the freshening of the 1950, early 1960 and mid 1980s, and the increase of salinity in the mid 1950s, early 1970s. Note that the fresh conditions of the 1990s are reproduced in contrast to failure of the scatter plot during this epoch. The prolonged southward flow anomalies lasted longer than the advection time from upstream boundary conditions and lead to a saturation of the salinity at fresh anomalies.

The correlation of the model and observations is 0.41, and explains approximately 17% of the variance. This skill is significant compared to the skill obtained by integration of equation (2) forced by random noise time series with the same lag-one autocorrelation as the observed velocities  $v'$ . Five thousand salinity reconstruction forced by noise yield a 95% significance level of the correlation of 0.36, with less than 2% correlated at a level higher than the reconstruction based on the observed velocity time series.

The quality of the fit is rather surprising considering the underlying assumptions:

The geostrophic flow estimates, based on coarse and irregular sampling, are likely contaminated by synoptic variations of the eddy rich eastern boundary region. Secondly, flow anomalies of line-90 might not be representative of anomalous advection in the upstream areas. And finally, the upstream boundary condition of constant anomalies might not be correct. In fact, recent observations reveal significant variations of salinity in the Alaska Gyre (Large 1996, Overland et al. 1999). How these observations relate to the source waters of the California Current is unknown.

## 6. Origins of the flow anomalies

The qualified skill of the anomalous advection hypothesis raises the question of the causes of the low-frequency anomalies of the California current. We investigate this question by studying the correlations of the observed geostrophic flow and pressure with the climate indices, and by exploring the relationship of the salinity and climate indices, when filtered as in equation (2). Consistent with the independence of the salinity signal with the climate indices (Fig. 8), both approaches indicated that ENSO, PDO, and the upwelling index account for only a small percentage of the variance of the velocity field. We are left with the tantalizing hypothesis that decadal anomalies of the California Current and strength of the salinity minimum result from forcing by unresolved atmospheric perturbations, or from forcing by synoptic ocean eddies that abound in this ocean area.

### 6.1. Analysis of ocean pressure

The geostrophic velocity anomalies in the area of the salinity minimum result from changes of ocean pressure at the inshore and offshore flanks. The time series of pressure in these two areas (Fig. 14) are very similar to  $S'_\rho$  in the halocline (Fig. 10). Inshore of the salinity minimum ocean pressure has a high correlation with ENSO (Table 1), with high pressure during El Niño, and low pressure during La Niña; offshore the correlation is much reduced. Compared to  $S'_\rho$ , the inshore and offshore anomalies of pressure have a higher correlation with  $PDO/SST$ , reflecting the large influence of surface temperature anomalies. The upwelling index shows also a modest effect on pressure, with stronger upwelling corresponding to lower pressure.

The geostrophic flow is the least robust of our results due the differencing operator and due to aliasing of the synoptic eddies by the sporadic observations. In the salinity minimum the flow corresponds to the difference of pressure in the coastal area and offshore (Fig. 14) and indicates northward current anomalies during the mid-1950s, early 1970s and early 1980s. Southward anomalies occurred during the early 1950s, early 1960s. Since the late 1980s and 1990s the California Current has intensified its southward flow (Di Lorenzo et al. 2004). Overall, the flow time series shows high variability that correlates neither with ENSO, PDO, nor the upwelling index (Table 1), for raw and smoothed evolutions.

Considering the EOFs of pressure yields a similar conclusion. For pressure along line 90, both the first and second principal components are correlated with El Niño, with

opposite effects on the California Current. The first EOF indicates a slowing during, in accordance to the Chelton et al. (1982) estimate of the leading EOF of steric height off the entire California Coast. The second EOF of line 90 pressure, however, suggests an acceleration. Together, the pressure EOFs yield an inconsistent relationship between El Niño and the cross-shore pressure gradient and suggest that the impact of El Niño on the California Current varies from event to event (Bograd et al. 2001).

## 6.2. Regression analysis of salinity

The lack of correlation of the flow with large scale indices suggests that its anomalies are either obscured by insufficient sampling, or are independent of the large scale climate anomalies. If anomalies of the California Current result from large-scale climate forcing, salinity anomalies due to long-shore advection are a linear combination of climate indices, smoothed and lagged by the temporal filter implied by long-shore advection (2),

$$S'(t) = \sum_j \beta_j \int_{t-\frac{y-y_0}{u}}^t dt' R_j(t') \quad (3)$$

where  $R_j$  are the large scale indices, and  $\beta_j$  are the regression parameters determined by least square fit. We investigate this hypothesis statistically (Chelton and Davis 1982), and consider as the large scale forcing indices NINO3.4, the PDO, and the upwelling index CCUP. The best fit model explains less than 5% of the salinity signal, whether we employ PDO/SST or PDO/AP.

The skill is worse than obtained from equation (2) forced with observed geostrophic flow anomalies  $v'$ , or obtained by fitting equation (3) to  $S'$  with  $R_j$  being the principal

components of ocean pressure from line 90. The latter reproduces the observed salinity evolution with a correlation of 0.5 (Fig. 13, light gray line), primarily due to the first principal component of pressure that accounts for 23% of the salinity variance. Note, however, that the variance this principal component shares with El Niño and PDO does not contribute to the skill of the fit.

The lack of correlation of the flow anomalies and salinity itself (Fig. 8) with the large scale indices, leads us to hypothesize that either unresolved, small-scale atmospheric wind-stress curl (Di Lorenzo 2003, Capet et al. 2004), or that the vigorous mesoscale variability in this region modulates the low frequency anomalies of the long-shore transport of the California Current, and thus controls the interannual and decadal evolution of salinity. Detailed modeling studies should be performed to explore these hypotheses.

## 7. Other processes

### 7.1. Surface fresh water flux

The trends of salinity averaged over the vertical extent of the anomalies from the surface to 150 m depth (Fig. 5) imply fresh water fluxes (Table 2) larger than observed anomalies of precipitation or evaporation. Multi-year precipitation anomalies would have to reach  $100 \text{ mm yr}^{-1}$  to  $200 \text{ mm yr}^{-1}$ , much larger than the observed 20 mm or smaller wet season (winter) anomalies in the coastal regions of North America (Dettinger et al. 1998). Latent heat flux anomalies would have to reach 10 to  $20 \text{ W m}^{-2}$ ,

again much larger than anomalies of the latent heat flux (Table 2) based on COADS observations (Cayan 1992). Thus, anomalies of precipitation or evaporation can not account for the observed changes of salinity.

## 7.2. River discharge

The Columbia and Fraser rivers discharge significant amounts of fresh water into the coastal ocean off Oregon and Strait of Juan de Fuca upstream of line 90. However, interannual anomalies are not large enough to account for the observed changes. The standard deviation of annual discharges of the Columbia and Fraser Rivers are  $1000 \text{ m}^3\text{s}^{-1}$  and  $350 \text{ m}^3\text{s}^{-1}$ , respectively (Dai and Trenberth 2002), with above average flow of the Columbia in the early 1970s, and below average flow in the late 1980 and early 1990s (Smith et al. 2001, their Fig. 15). In addition to being inconsistent with the changes of salinity during these time periods, a river discharge anomaly of  $2000 \text{ m}^3\text{s}^{-1}$ , diluted over the California current with a depth of 150 m, a width of 300 km and a southward speed of  $2 \text{ cm s}^{-1}$ , changes salinity by 0.08 psu only, smaller than the observed anomalies (Fig. 13).

## 7.3. Upstream cross-shore exchanges

Upstream anomalies of the cross-shore exchange processes can not be entirely excluded based on the line-90 data if, by the time waters reach line-90, adjustments have neutralized density perturbations while conserving the salinity perturbation. On seasonal time scales, the formation of seasonal equatorward jet leads to instabilities and

eddies that move offshore and transport coastal waters into the subtropical gyre (Kelly et al. 1998) and provide an important heating of the coastal waters (Marchiesiello et al. 2003). We speculate that a similar transport of salt by synoptic processes takes place, so that anomalies of eddy activity alter the lateral flux of salt and the strength of the salinity minimum. It remains to be investigated in future modeling studies, how the dynamical adjustment of the ocean and atmospheric boundary layers affect interannual anomalies of salinity and density downstream at line-90.

## 8. Conclusions

Temperature and salinity in the California Current have very different low frequency variability. The leading signal of temperature is dominated by interannual time-scales, and shows a warming trend that commenced in the 1980s (Roemmich and McGowan 1995). The temperature variations are correlated with ENSO, and are coherent with the Pacific Decadal Oscillation (PDO).

The variability of salinity is dominated by decadal time scales, with changes of order of 0.2 psu, and fresh conditions in the early 1950s, from 1966 to 1971, in 1978 and in the early 1990s. Salinity was anomalous high in the late 1930s, from 1956 to 1965, in the mid 1970s, and around 1990. This variability is independent of the large-scale climate indices of ENSO and the PDO, of temperature variability, and of anomalies of halocline depth that are correlated with ENSO.

The salinity variability results from anomalous long-shore advection that is accumulated along the equatorward trajectory of water in the California Current.

Other forcing such as surface fresh water flux, vertical mixing, vertical advection, and lateral exchanges are either too small to account for the observed changes, or imply a correlation of variations of salinity and density, inconsistent with the observed lack of associated low-frequency salinity and density signals.

Since the interannual and decadal long-shore flow anomalies of the California Current are independent of the large scale climate indices, we hypothesize that unresolved, small-scale wind stress curl, or intrinsic ocean mesoscale variations, prevalent in the California Current (e.g. Di Lorenzo 2003), randomly accelerate or slow the long-shore flow. Variations in the upstream cross-shore eddy salt transports could be an alternative generation mechanism for the low-frequency salinity anomalies, provided that adjustment processes diminish the associated density perturbation, while conserving the salinity anomalies. Clearly, the role of eddies in the decadal anomalies of salinity and long-shore flow needs to be clarified, and provide a rich area for analysis and experiments with high resolution numerical models.

One additional piece of evidence for the accumulation along flow trajectories of long-shore advection anomalies stems from observation of plankton abundance in the California Current. Chelton et al. (1982, their Fig. 5) show that the dominant frequency of non-seasonal zooplankton concentrations, related to anomalies of along-shore advection, increases toward the south, from primarily interannual periods off San Francisco to decadal periods off Baja. This is consistent with anomalous advection, spatially coherent along the coast and with a white frequency spectrum, being accumulated along the southward trajectory in the California Current.

Why do temperature and salinity have such distinct dominant variability? The preponderance of salinity variance at low frequencies results from a lack of negative feedback acting on surface salinity anomalies – the surface fresh water flux and other terms of the salinity budget are independent of oceanic salinity anomalies. This is in contrast to temperature variance that is bounded by feedbacks of the air-sea heat flux, and by its control of ocean density and dynamics. In addition, the climatological fields of temperature and salinity in the California Current suggest that the ratio of horizontal to vertical advection is larger for salinity than for temperature. In the California current between 30°N and 40°N (Fig. 1), and between depths of 50m and 100m (Figs. 4), time-mean temperature varies by 4°K in the horizontal, and 5°K in the vertical, while time-mean salinity varies by 0.8psu in the horizontal, and only 0.3 psu in the vertical. Thus, the ratio of long-shore to vertical gradients of mean salinity is nearly three times that of mean temperature. This implies that temperature is mostly affected by vertical processes, while for salinity lateral advection dominates.

In models, the lack of feedback between air-sea fresh water flux and surface salinity implies that any errors of the salt budget lead to erroneous storage. However, the common surface boundary condition of relaxing surface salinity to observations artificially limits the low frequency variance. This poses a major challenge to ocean models that attempt to simulate low frequency variations. This is particularly important since salinity anomalies in the California current might affect eastern subtropical mode water (Hautala and Roemmich 1998), that is formed in the low density gradient regions off the coast of California and Baja (Hosoda et al. 2001). This suggest that the

primarily low frequency salinity anomalies in the California Current are subducted into the thermocline, and could play a role in decadal climate anomalies of the Pacific.

**Acknowledgment.** The authors thank Drs. Bruce Cornuelle, Arthur J. Miller, David W. Pierce and Jim Potemra for helpful discussions and comments on the manuscript. This paper is funded by the National Science Foundation (OCE00-82543) and the Department of Energy (DE-FG03-01ER63255). The views expressed herein are those of the authors and do not necessarily reflect the views of NSF or DOE or any of their sub-agencies. This is IPRC contribution XXXX and SOEST contribution XXXX.

## References

- Bakun, A., 1990: Global climate change and intensification of coastal ocean upwelling. *Science*, **247**, 198-201.
- Bograd, S. J., T. K. Chereskin and D. Roemmich, 2001: Transport of mass, heat, salt, and nutrients in the southern California Current system: Annual cycle and interannual variability. *J. Geophys. Res.*, **106**, 9255-9275.
- Bograd, S. J. and R. J. Lynn, 2003: Long term variability in the Southern California Current system. *Deep-Sea Res. II*, **50**, 2355-2370.
- Bindoff, N. L. and T. J. McDougall, 1994: Diagnosing climate change and ocean ventilation using hydrographic data. *J. Phys. Oceanogr.*, **24**, 1137-1152.
- Bray, N. A., A. Keyes, et al., 1999: The California Current system in the Southern California Bight and the Santa Barbara channel. *J. Geophys. Res.*, **104**, 7695-7714.
- Capet, X. J., P. Marchesiello and J. C. McWilliams, 2004: Upwelling response to coastal wind profiles. *Geophys. Res. Lett.*, **31**, L12211, doi:10.1029/2004GL020123.
- Cayan, D. R., 1992: Variability of latent and sensible heat fluxes estimated using bulk formulae. *Atmos.-Ocean.*, **30**, 1-42.
- Chelton, D. B., 1981: Interannual variability of the California Current – Physical factors. *CalCoFI Rep.*, **XXII**, 34-48.
- Chelton, D. B., and R. E. Davis, 1982: Monthly mean sea-level variability along the west coast of North America. *J. Phys. Oceanogr.*, **12**, 757-784.
- Chelton, D. B., P. A. Bernal and J. A. McGowan, 1982: Large-scale interannual physical and biological interaction in the California Current. *J. Mar. Res.*, **40**, 1095-1125.

- Church, J. A., J. S. Godfrey, D. R. Jackett, and T. J. McDougal, 1991: A model of sea level rise caused by ocean thermal expansion. *J. Climate*, **4**, 438-345.
- Clarke, A. J., and A. Lebedev, 1999: Remotely driven decadal and longer changes in the coastal Pacific waters of the Americas. *J. Phys. Oceanogr.*, **29**, 828-835.
- Cornuelle, B. D., T. K. Chereskin, P. P. Niiler, M. Y. Morris and D. K. Musgrave, 2000: Observations and modeling of a California undercurrent eddy. *J. Geophys. Res.*, **105**, 1227-1243.
- Dai, A. and K. E. Trenberth, 2002: Estimates of freshwater discharge from continents: Latitudinal and seasonal variations. *J. Hydrometeorology*, **3**, 660-687.
- Davis, R. E., 1976: Predictability of sea surface temperature and sea level pressure anomalies over the North Pacific Ocean. *J. Phys. Oceanogr.*, **6**, 249-266.
- Dettinger, M. D., D. R. Cayan, H. F. Diaz and D. M. Meko, 1998: North-south precipitation patterns in western North America on interannual-to-decadal timescales. *J. Clim.*, **11**, 3095-3111.
- Di Lorenzo, E., 2003: Seasonal dynamics of the surface circulation in the Southern California Current System. *Deep Sea Res., II*, **50**, 2371-2388.
- Di Lorenzo, E., A. J. Miller, N. Schneider and J. C. McWilliams, 2004: The warming of the California Current system: Dynamics, thermodynamics and ecosystem implications. *J. Phys. Oceanogr.*, **XX**, in press.
- Emery, W.J. and K. Hamilton, 1985: Atmospheric forcing of interannual variability in the Northeast Pacific-Ocean – Connections with El-Niño. *J. Geophys. Res.*, **90**, 857-868.

- Hall, A. and S. Manabe, 1997: Can local stochastic theory explain sea surface temperature and salinity variability?. *Clim. Dyn.*, **13**, 167-180.
- Hautala, S. L. and D. H. Roemmich, 1998: Subtropical mode water in the Northeast Pacific basin. *J. Geophys. Res.*, **103**, 13,055-13,066.
- Hasselmann, K., 1976: Stochastic climate models. Part 1. Theory. *Tellus*, **26**, 473-485.
- Hickey, B. M., 1979: The California Current system: Hypothesis and facts.. *Prog. Oceanogr.*, **8**, 191-279.
- Hosoda, S., S.-P. Xie, K. Takeuchi and M. Nonaka, 2001: Eastern North Pacific Subtropical Model Water in a general circulation model: Formation mechanism and salinity effects. *J. Geophys. Res.*, **106**, 19,671-19,681.
- Kelly KA, Beardsley RC, Limeburner R, Brink KH, Paduan JD, Chereskin TK, 1998: Variability of the near-surface eddy kinetic energy in the California Current based on altimetric, drifter, and moored current data. *J. Geophys. Res.*, **103**, 13067-13083.
- Large, W. G., 1996: An observational and numerical investigation of the climatological heat and salt balances at OWS Papa. *J. Clim.*, **9**, 1856-1876.
- Levitus, S., T.P. Boyer, M.E. Conkright, T. O'Brien, J. Antonov, C. Stephens, L. Stathoplos, D. Johnson, and R. Gelfeld, 1998: NOAA Atlas NESDIS 18, WORLD OCEAN DATABASE 1998: Vol. 1: Introduction. *U.S. Gov. Printing Office, Wash., D. C.*, **Vol. 1**, 346 pp.
- Lluch-Cota, D. B., W. S. Wooster and S. R. Hare, 2001: Sea surface temperature variability in coastal areas of the Northeastern Pacific related to the El Niño-Southern Oscillation and the Pacific Decadal Oscillation. *Geophys. Res. Lett.*, **28**, 2029-2032.

- Lynn, R. J., and J.J. Simpson, 1987: The California Current system: the seasonal variability of its physical characteristics. *J. Geophys. Res.*, **92**, 12947-12966.
- Lynn, R. J. and S. J. Bograd, 2002: Dynamic evolution of the 1997-1999 El Niño-La Niña cycle in the southern California Current System. *Prog. Oceanogr.*, **54**, 59-75.
- Mantua, N.J, S.R. Hare, Y. Zhang, J. M. Wallace, and R.C. Francis, 1997: A Pacific interdecadal climate oscillation with impacts on salmon production. *Bull. Am. Met. Soc.*, **78**, 1069-1079.
- Marchiesiello, P., J. C. McWilliams and A. Shchepetkin, 2003: Equilibrium structure and dynamics of the California Current system. *J. Phys. Oceanogr.*, **33**, 753-783.
- McGowan, J. A., D. R. Cayan and L. M. Dorman, 1998: Climate-ocean variability and ecosystem response in the Northeast Pacific. *Science*, **281**, 210-217.
- Miller, A. J., Cayan, D. R., Barnett, T. P., Graham, N. E., and Oberhuber, J. M., 1994: Interdecadal variability of the Pacific Ocean: Model response to observed heat flux and wind stress anomalies. *Clim. Dyn*, **9**, 287-302..
- Miller, A.J., J.C. McWilliams, N.Schneider, J.S. Allen, J.A. Barth, R.C. Beardsley, T. Chereskin, C.A. Edwards, R. Haney, K.A. Kelly, J. Kindle, L. Ly, J. Moisan, M. Noble, P.P. Niiler, L.Y. Oey, F. Schwing, K. Shearman, and M.S. Swenson, 1999: Observing and modeling the California current system: Purposes, achievements and aspirations. *EOS*, **80**, 533-539, (7 pp.).
- Overland, J. E, S. Salo and J. M. Adams, 1999: Salinity signature of the Pacific Decadal Oscillation. *Geophys. Res. Lett.*, **26**, 1337-1340.

- Ramp, S. R., J. L. McClean, C. A. Collins, A. J. Semtner and K. A. S. Hayes, 1997: Observations and modeling of the 1991-1992 El Niño signal off central California. *J. Geophys. Res.*, **102**, 5553-5582.
- Roemmich, D. and J. McGowan, 1995: Climatic warming and the decline of zooplankton in the California Current. *Science*, **267**, 1324-1326.
- Roemmich, D., 1992: Ocean warming and sea level rise along the southwest U.S. coast. *Science*, **257**, 373-375.
- Roemmich, D., 1989: Mean transport of mass, heat, salt and nutrients in southern California coast waters: implications for primary production and nutrient cycling. *Deep-Sea Res.*, **36**, 1359-1378.
- Schneider, N., and B. D. Cornuelle, 2004: The forcing of the Pacific Decadal Oscillation. *J. Climate*, **XX**, submitted.
- Schwing, F. B., and R. Mendelssohn, 1997: Increased coastal upwelling in the California Current. *J. Geophys. Res.*, **102**, 3421-3438.
- Schwing, F. B., T. Murphree, L. DeWitt and P. Green, 2002: The evolution of oceanic and atmospheric anomalies in the northeast Pacific during the El Niño and La Niña events of 1995-2000. *Prog. Oceanogr.*, **54**, 459-491.
- Simpson, J. J., 1992: Response of the Southern California current system to the mid-latitude North Pacific coastal warming events of 1982-1983 and 1940-1941. *Fish. Oceanogr.*, **1**, 57-79.
- Smith, R. L., A. Huyer and J. Fleischbein, 2001: The coastal ocean of Oregon from 1961-2000: Is there evidence of climate change or only of Los Niños?. *Prog. Oceanogr.*, **49**, 63-93.

Swenson, M. S. and P. P. Niiler, 1996: Statistical analysis of the surface circulation of the California Current. *J. Geophys. Res.*, **101**, 22,631–22,645.

Trenberth, K. E., 1990: Recent observed interdecadal climate changes in the Northern Hemisphere. *Bull. Am. Met. Soc.*, **71**, 988-993.

Trenberth, K. E. and J. W. Hurrell, 1994: Decadal atmosphere-ocean variations in the Pacific. *Clim. Dyn.*, **9**, 303-319.

Zhang, Y., J.M. Wallace and D.S. Battisti, 1997: ENSO-like interdecadal variability: 1900-93. *J. Clim.*, **10**, 1004-1020.

---

## Figure Captions

**Fig. 1.** Climatological salinity in psu (left), surface temperature in °C (center), and density in  $\text{kg m}^{-3}$  (right). Data are from the Levitus et al. (1998) climatology. Symbols mark the station locations of CalCoFI line-90. The white line shows the position of the nominal line-90.

**Fig. 2.** Total number of hydrographic stations per year. Shading shows the stations in three areas: east of  $120^\circ\text{W}$  (dark shade), between  $122.5^\circ$  and  $120^\circ\text{W}$  (medium shade) and west of  $122.5^\circ\text{W}$  (light shade).

**Fig. 3.** Salinity in psu at the surface along line-90 data as a function of longitude and time. Scale of salinity is given in color scale on the right. Dots mark positions of observations. Original data have been optimally interpolated onto a nominal line as shown in Figure 1. White areas have insufficient data coverage.

**Fig. 4.** Line 90 climatology of (top) temperature in °C, (center) salinity in psu, and (bottom) geostrophic velocity normal to line-90 in  $\text{cm s}^{-1}$  as a function of longitude and depth in meters. Geostrophic flow has been estimated relative to 500 m depth. Positive numbers correspond to northward flows. The coast is on the right in all panels.

**Fig. 5.** Leading EOF of salinity anomalies at CalCoFI line-90. Top panel shows the principal component. The bottom panel shows the spatial loading pattern, in units of psu. Contour level is 0.02 psu and shading is shown by the bar on the right. This EOF accounts for 38% of the variance of the seasonal salinity anomalies.

**Fig. 6.** Same as Fig. 5, but for temperature anomalies at CalCoFI line-90. Contour interval in the bottom panel is 0.2 °K. The EOF accounts for 47% of the variance of the seasonal temperature anomalies.

**Fig. 7.** Frequency spectrum of leading EOFs of temperature (gray) and salinity (black) anomalies. Spectra were estimated by least square fit of the Fourier components to the data, and smoothed by the running average of 8 adjacent frequencies. The error bars are the standard errors of the averaged powers, and are only shown every 3rd frequency. For reference, a '-2' frequency slope is indicated in dark gray.

**Fig. 8.** Lagged correlation of the leading EOFs of temperature (left) and salinity (right) anomalies with tropical Pacific surface temperatures anomalies (NINO3.4, solid), and with the Pacific Decadal Oscillation (PDO, dotted) and with the upwelling index of central California (CCUP, dashed). Note that the sign of indices have been reversed when indicated by a minus sign. Negative lags (in months) indicate that indices lead variations off California.

**Fig. 9.** Variance of anomalies of salinity in psu. Top panel shows root-mean-square (rms) value of anomalies of salinity, the center panel shows the rms of anomalies of salinity associated with vertical displacements of isopycnals, and the lower panel shows the rms of salinity variations independent of density.

**Fig. 10.** Time series of salinity  $S'_\rho$  associated with density variations (halocline heave) in psu at depth from 100 to 200m. Top line shows variations east of 121.5°W ('Coast'), bottom from west of 121.5°W ('Offshore'). The top panel has been offset by 0.3 psu, zero anomalies are denoted by thin lines. Thin dotted lines in the upper panel denote El Niño (downward) and La Niña (upward) events.

**Fig. 11.** (Top) Salinity and (bottom) along-shore geostrophic current in the salinity minimum, averaged from the surface to a depth of 50 m. Thick gray lines mark average rate of change of salinity (top) and mean geostrophic (bottom) during epochs chosen for consistent salinity trend. Positive currents correspond to poleward flows. The thin gray line (top) marks the salinity variations averaged over the top 150 m of the water column.

**Fig. 12.** Scatter plot of epoch averages of geostrophic velocity and rate of change of salinity. Epochs are as shown in Fig. 11 and are indicated by their center year. Error bars denote 90% confidence intervals. The climatological along-shore salinity gradient of 0.3 psu/1000 km (Fig. 1) is shown as a dashed line, and is consistent with the along-shore advection hypothesis in the 1950s, 1960s, and 1980s.

**Fig. 13.** Salinity in the salinity minimum from seasonal line 90 data (black line), expected from equation (2) forced by anomalous advection (dark gray), and least square fit of salinity variations to equation (3) forced by line-90 pressure EOFs (thick, light gray line).

**Fig. 14.** Time series of ocean pressure relative to 500 m east (top, 'Coast') and west (bottom, 'Offshore') of 121.2°W, and averaged over the top 50 m of the water column. Pressure has been normalized to units of  $\text{cm s}^{-1}$  by the local Coriolis frequency, and the distance between the regions. The difference is displayed in the center panel, and is the along-shore geostrophic current, with positive numbers indicating poleward flow. The thin dotted vertical lines in the top plot denote El Niño (upward) and La Niña (downward) events.

		NINO3.4	<i>PDO/SST</i>	<i>PDO/AP</i>	<i>CCUP</i>
$S'_\rho$	Coast	-0.48 -1	-0.24 -3	-0.15 0	0.26 2
		(-0.66) -5	(-0.42) -10	(0.45) -9	(0.40) -3
	Offshore	-0.25 -1	-0.28 -10	0.11 -10	0.14 -2
		(-0.51) -11	(-0.36) -11	(0.40) -10	(0.23) -12
$P'$	Coast	0.60 -1	0.42 0	-0.25 0	-0.41 -2
		(0.74) -5	(0.61) -1	(-0.63) -9	(-0.45) -3
	Offshore	0.29 -5	0.37 -4	-0.17 -5	-0.25 -2
		(0.64) -1	(0.59) -10	(-0.61) -9	(-0.48) -3
$V'_{GEOS}$		0.20 -3	-0.23 10	0.18 8	0.16 7
		(-0.37) 10	(-0.28) -9	(0.3) -8	(0.25) 10

**Table 1.** Correlation of NINO3.4, PDO and CCUP indices with anomalies  $S'_\rho$  in the halocline (100 to 200 m depth), and pressure at the surface (0 to 50 m depth), east ('Coast') and west ('Offshore') of 125.5°W. Integer numbers indicate the lag in month when this correlation occurs, with negative lags indicating lead of the large scale index. Correlations are calculated from seasonal data. The bottom row shows the correlation of the geostrophic flow anomalies between 122.5° and 120°W and surface to 50 m depth. Values in parenthesis result after smoothing the time series with a 13 season filter, with linearly varying weights.

	1949-53	1953-58	1958-62	1962-70	1970-75	1981-90	1990-2002
$10^{-2}$ psu yr $^{-1}$	-2.6	4.7	0.4	-2.2	5.5	-1.8	0.7
$\partial_t S'$ mm yr $^{-1}$	115	-205	-17	95	-245	81	-32
W m $^{-2}$	-9	16	1.4	-8	19	-6	-3
$Q_{lat}^{COADS}$ W m $^{-2}$ , 35°N	-3.3	-0.4	1.6	1.1	-0.2	-2.9	2.9
$Q_{lat}^{COADS}$ W m $^{-2}$ , 40°N	-2.8	-0.7	5.5	1.9	-3.7	-0.8	2.7
$V'_{GEOS,500m}$ cm s $^{-1}$	-1.4	0.5	-0.1	-0.8	0.3	-0.9	-1.6

**Table 2.** Epoch averages of the salinity storage in units of  $10^{-2}$  psu/yr for data from 122.5°W to 120°W, surface to 150 m depth. Second and third rows show the implied surface fresh water and heat fluxes required to attain these trends in a layer of 150 m thickness. The bottom rows show the latent heat flux at 125°W, 35°N and 120°W, 40°N observations (Cayan 1992), and the geostrophic flow, estimated relative to 500 m from the hydrographic data. Positive fresh water fluxes correspond to increased precipitation, positive latent heat fluxes corresponds to a transfer of latent heat (and fresh water) from the ocean to the atmosphere, and positive long-shore velocities correspond to poleward anomalies.

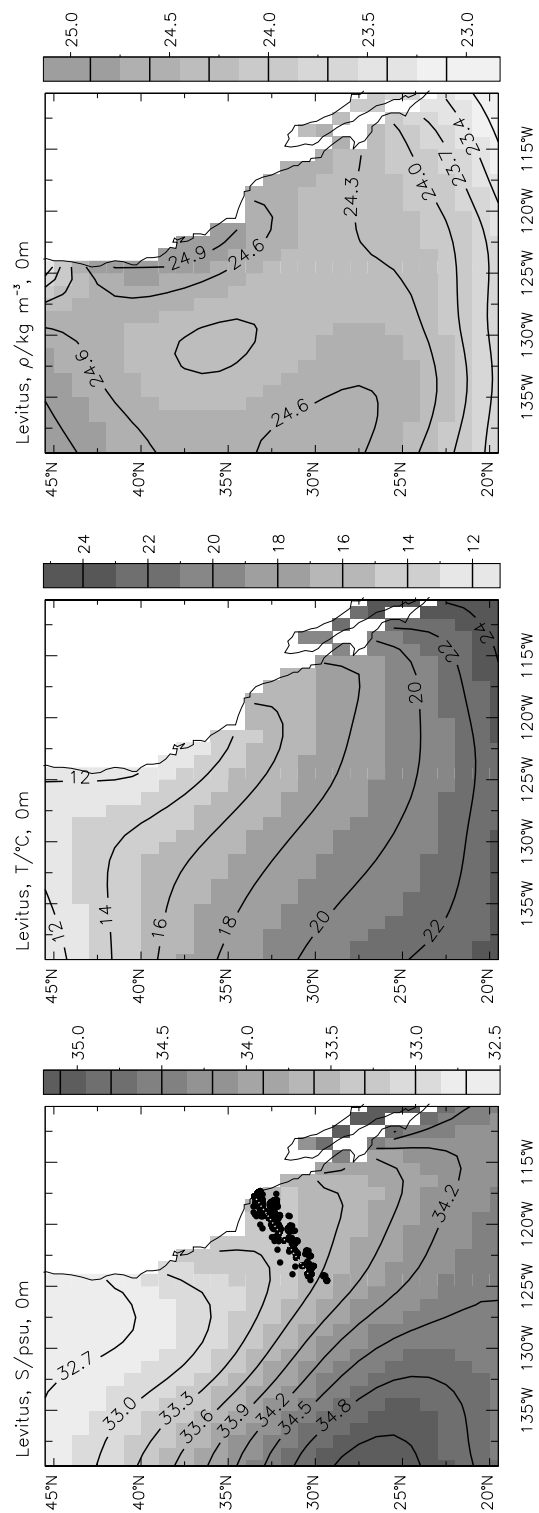


**Fig. 1.** Climatological salinity in psu (left), surface temperature in  $^{\circ}\text{C}$  (center), and density in  $\text{kg m}^{-3}$  (right). Data are from the Levitus et al. (1998) climatology. Symbols mark the station locations of CalCoFI line-90. The white line shows the position of the nominal line-90.

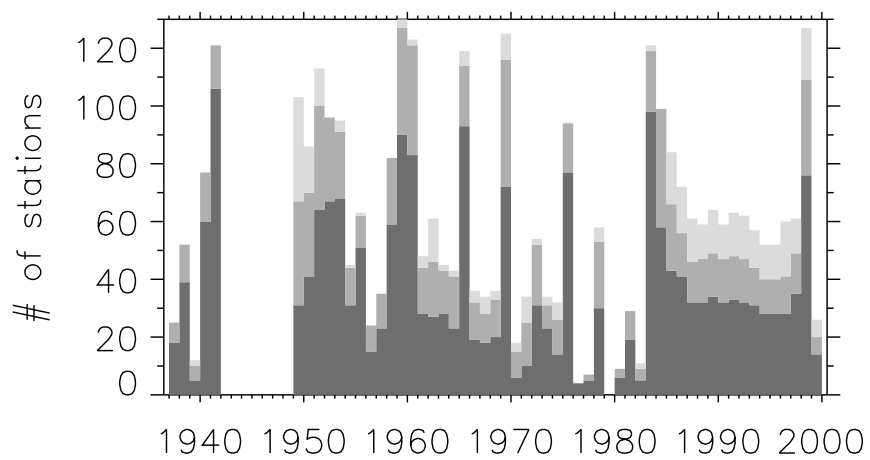


**Fig. 2.** Total number of hydrographic stations per year. Shading shows the stations in three areas: east of 120°W (dark shade), between 122.5° and 120°W (medium shade) and west of 122.5°W (light shade).

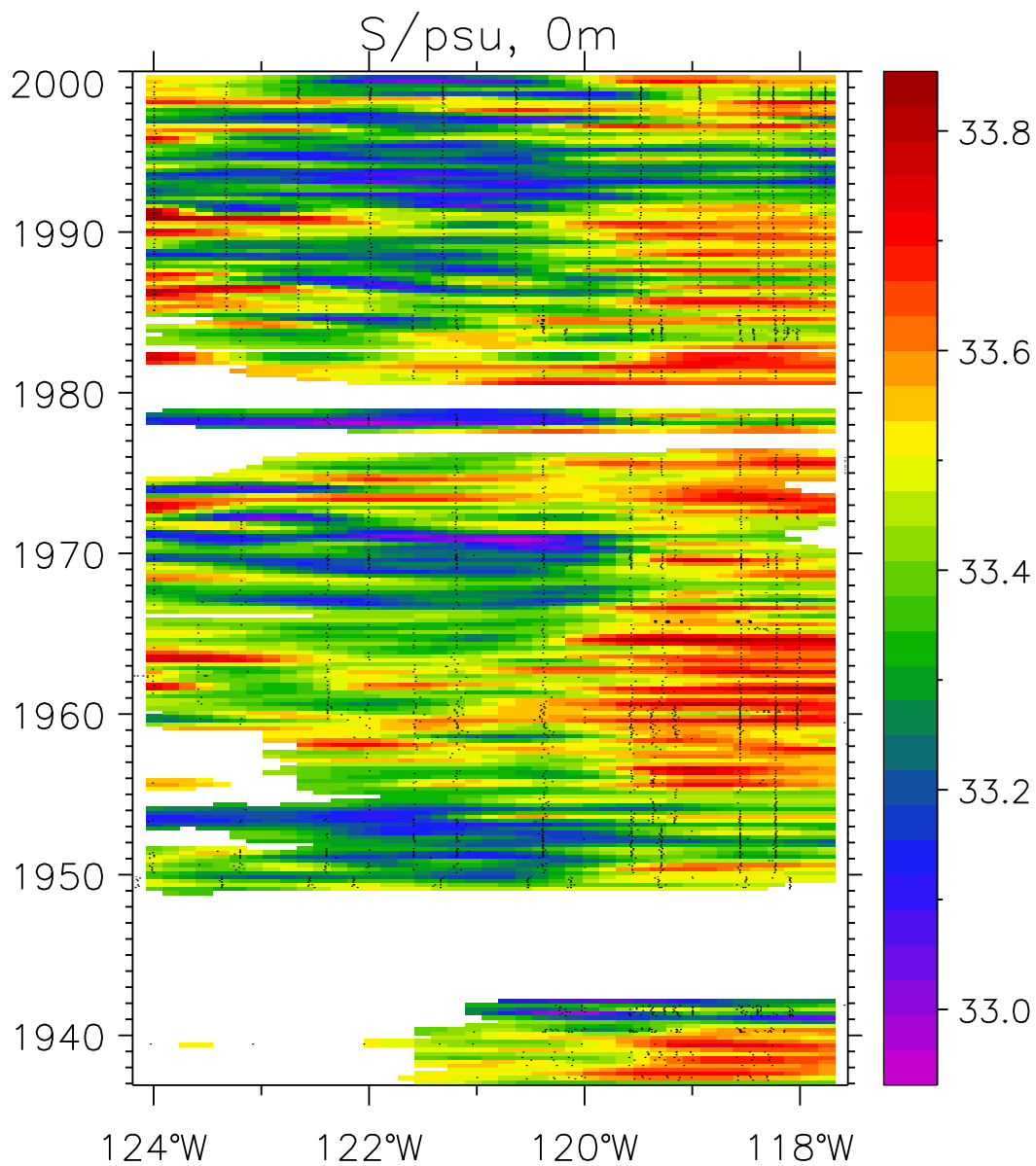


**Fig. 3.** Salinity in psu at the surface along line-90 data as a function of longitude and time. Scale of salinity is given in color scale on the right. Dots mark positions of observations. Original data have been optimally interpolated onto a nominal line as shown in Figure 1. White areas have insufficient data coverage.

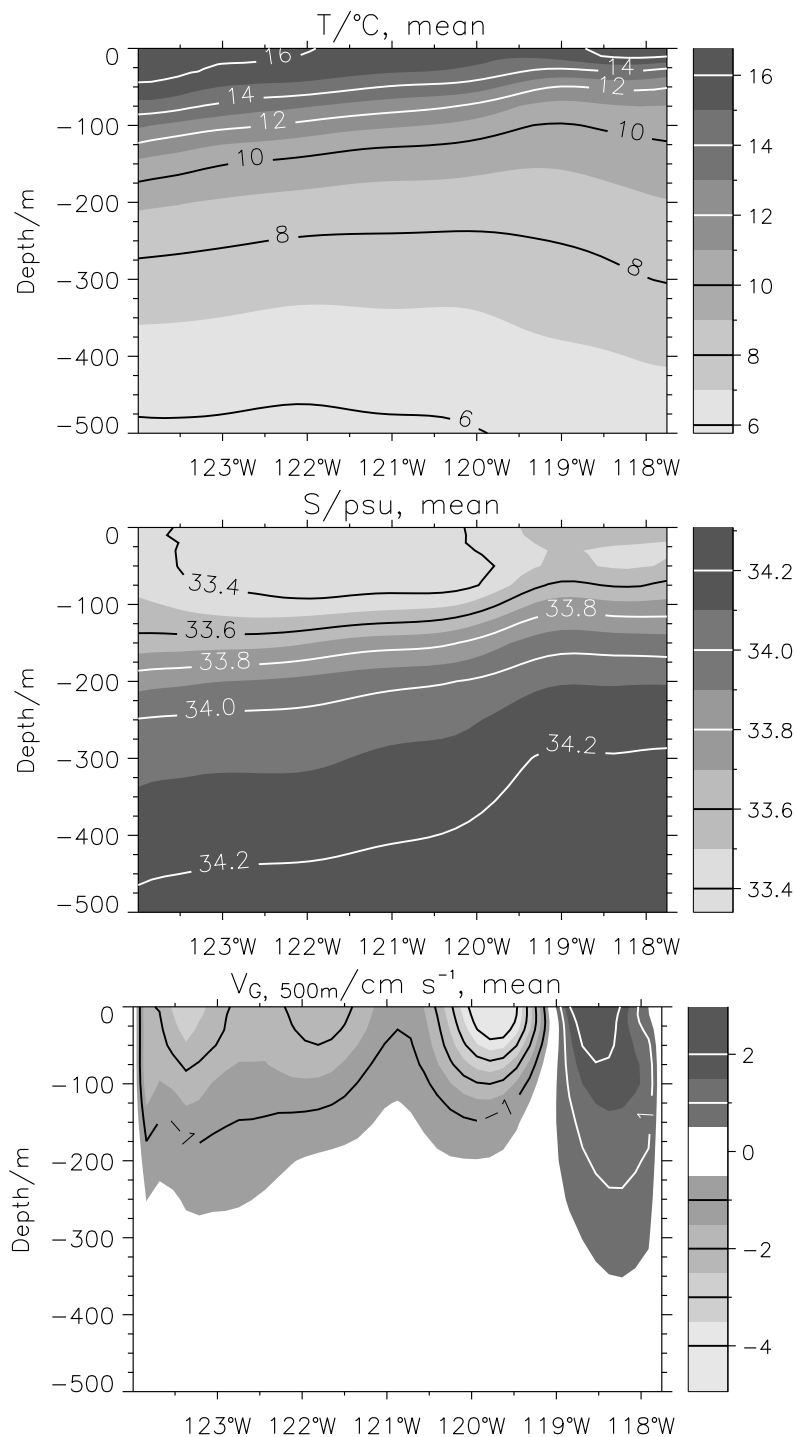


**Fig. 4.** Line 90 climatology of (top) temperature in  $^\circ\text{C}$ , (center) salinity in psu, and (bottom) geostrophic velocity normal to line-90 in  $\text{cm s}^{-1}$  as a function of longitude and depth in meters. Geostrophic flow has been estimated relative to 500 m depth. Positive numbers correspond to northward flows. The coast is on the right in all panels.

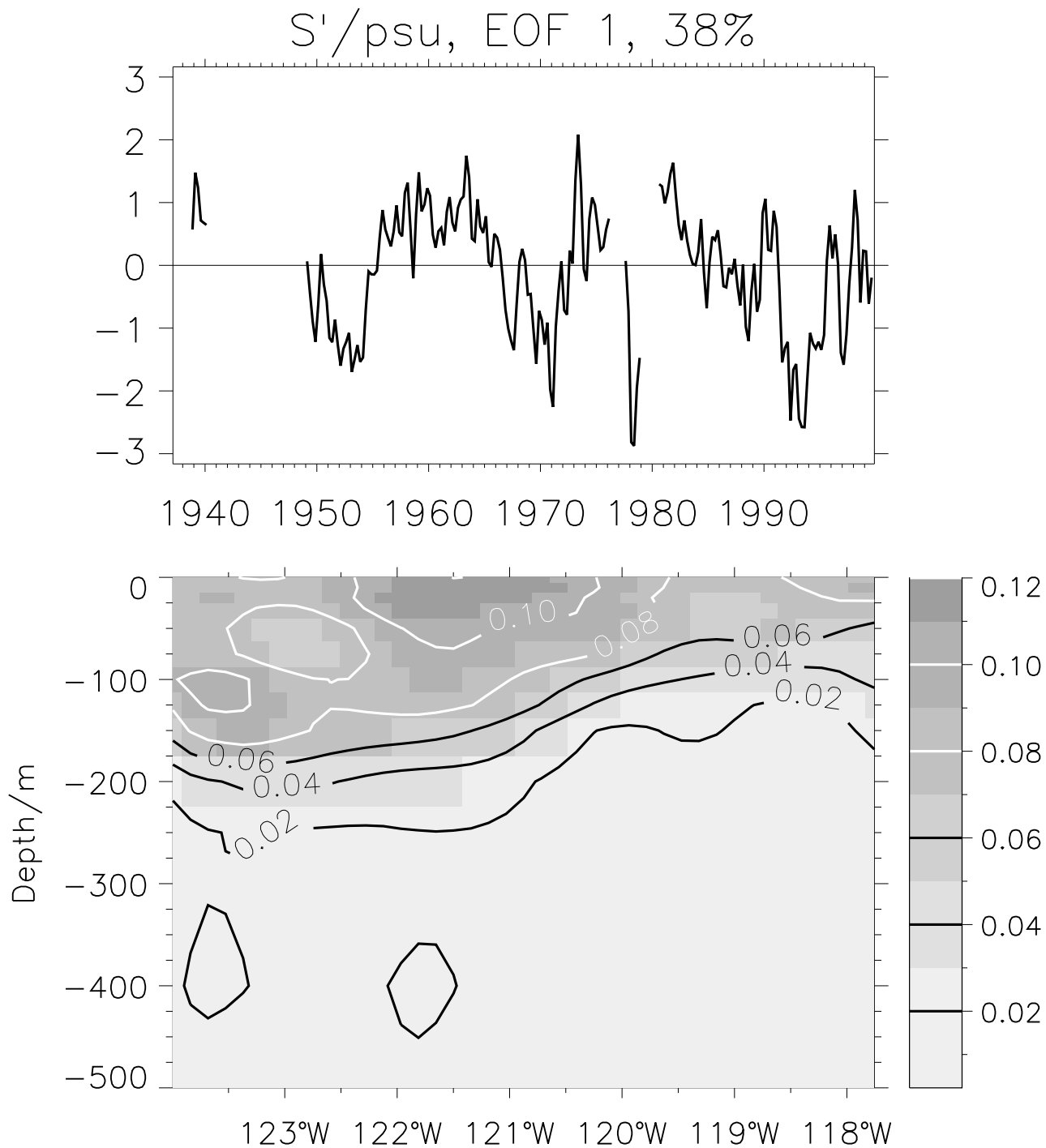


**Fig. 5.** Leading EOF of salinity anomalies at CalCoFI line-90. Top panel shows the principal component. The bottom panel shows the spatial loading pattern, in units of psu. Contour level is 0.02 psu and shading is shown by the bar on the right. This EOF accounts for 38% of the variance of the seasonal salinity anomalies.

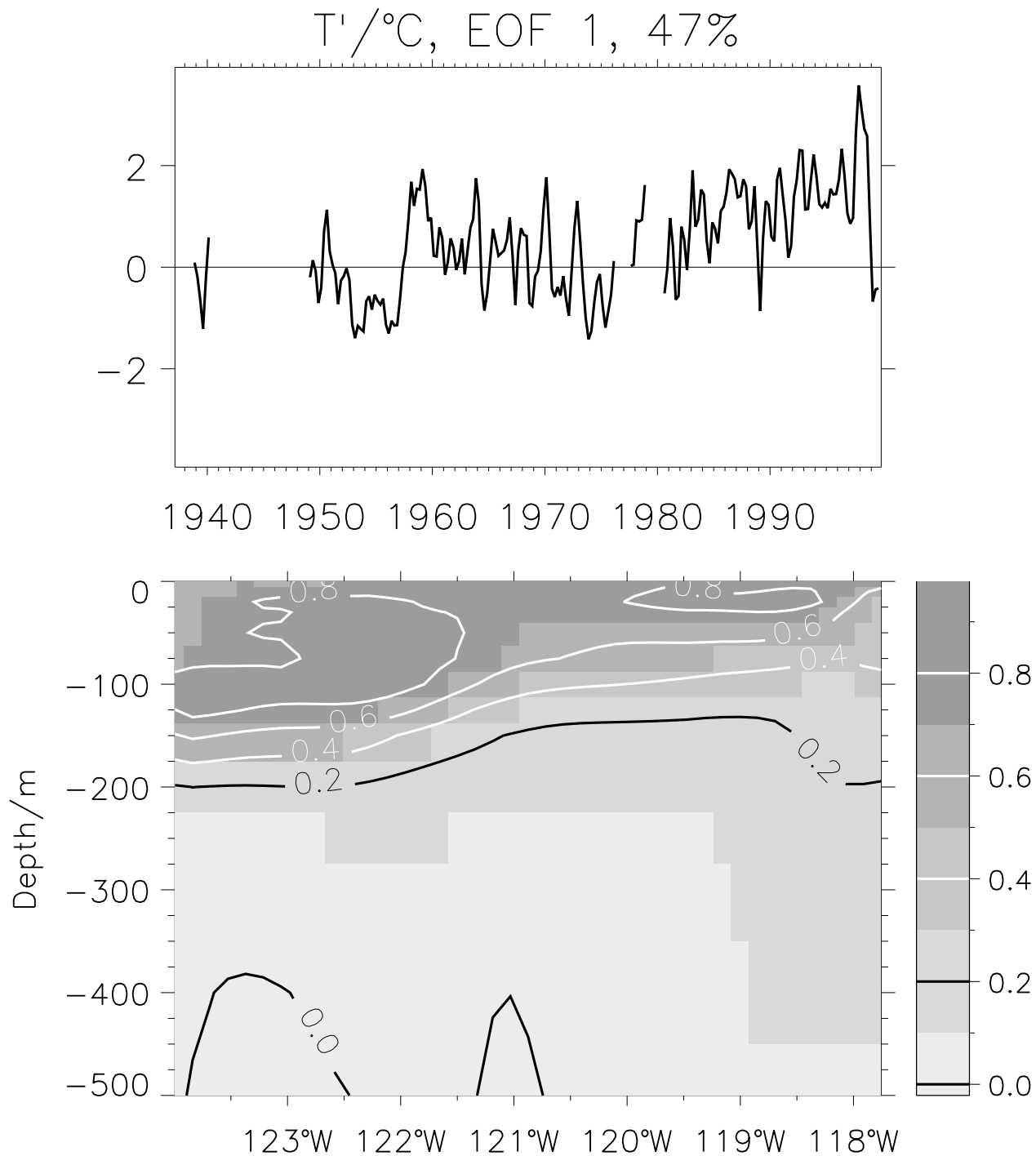


**Fig. 6.** Same as Fig. 5, but for temperature anomalies at CalCoFI line-90. Contour interval in the bottom panel is 0.2 °K. The EOF accounts for 47% of the variance of the seasonal temperature anomalies.

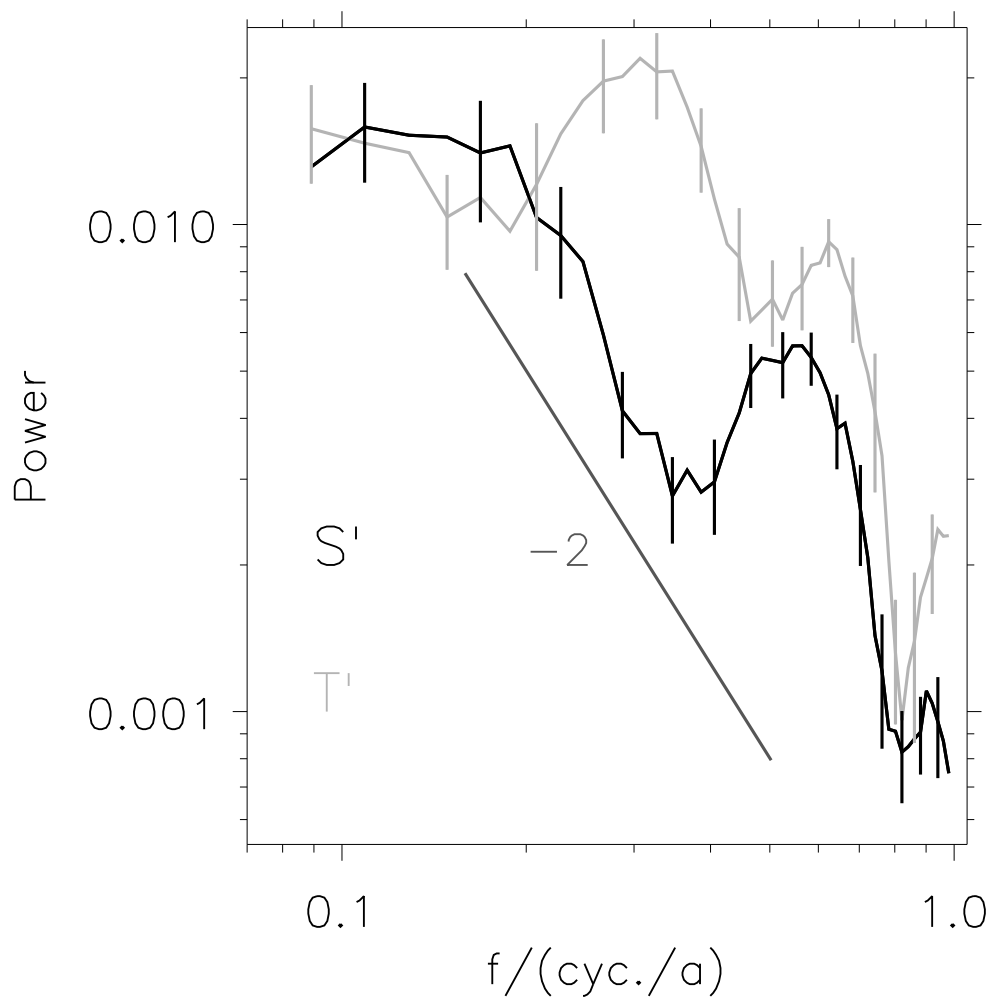


**Fig. 7.** Frequency spectrum of leading EOFs of temperature (gray) and salinity (black) anomalies. Spectra were estimated by least square fit of the Fourier components to the data, and smoothed by the running average of 8 adjacent frequencies. The error bars are the standard errors of the averaged powers, and are only shown every 3rd frequency. For reference, a '-2' frequency slope is indicated in dark gray.

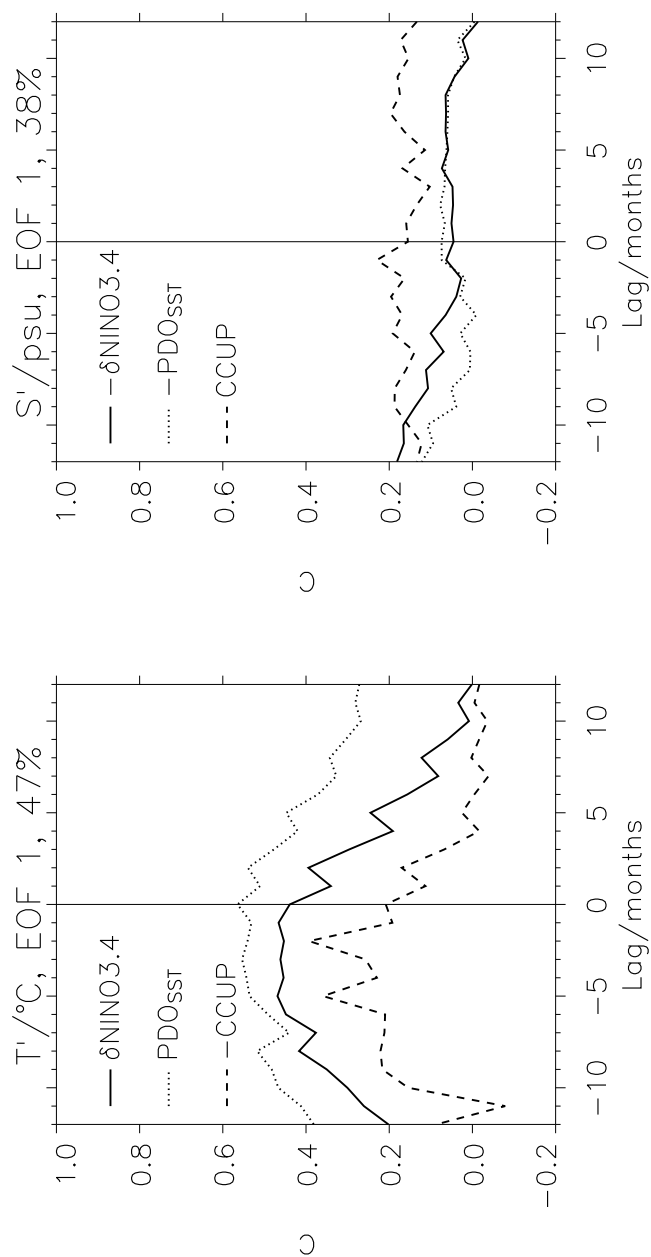


**Fig. 8.** Lagged correlation of the leading EOFs of temperature (left) and salinity (right) anomalies with tropical Pacific surface temperatures anomalies (NINO3.4, solid), and with the Pacific Decadal Oscillation (PDO, dotted) and with the upwelling index of central California (CCUP, dashed). Note that the sign of indices have been reversed when indicated by a minus sign. Negative lags (in months) indicate that indices lead variations off California.

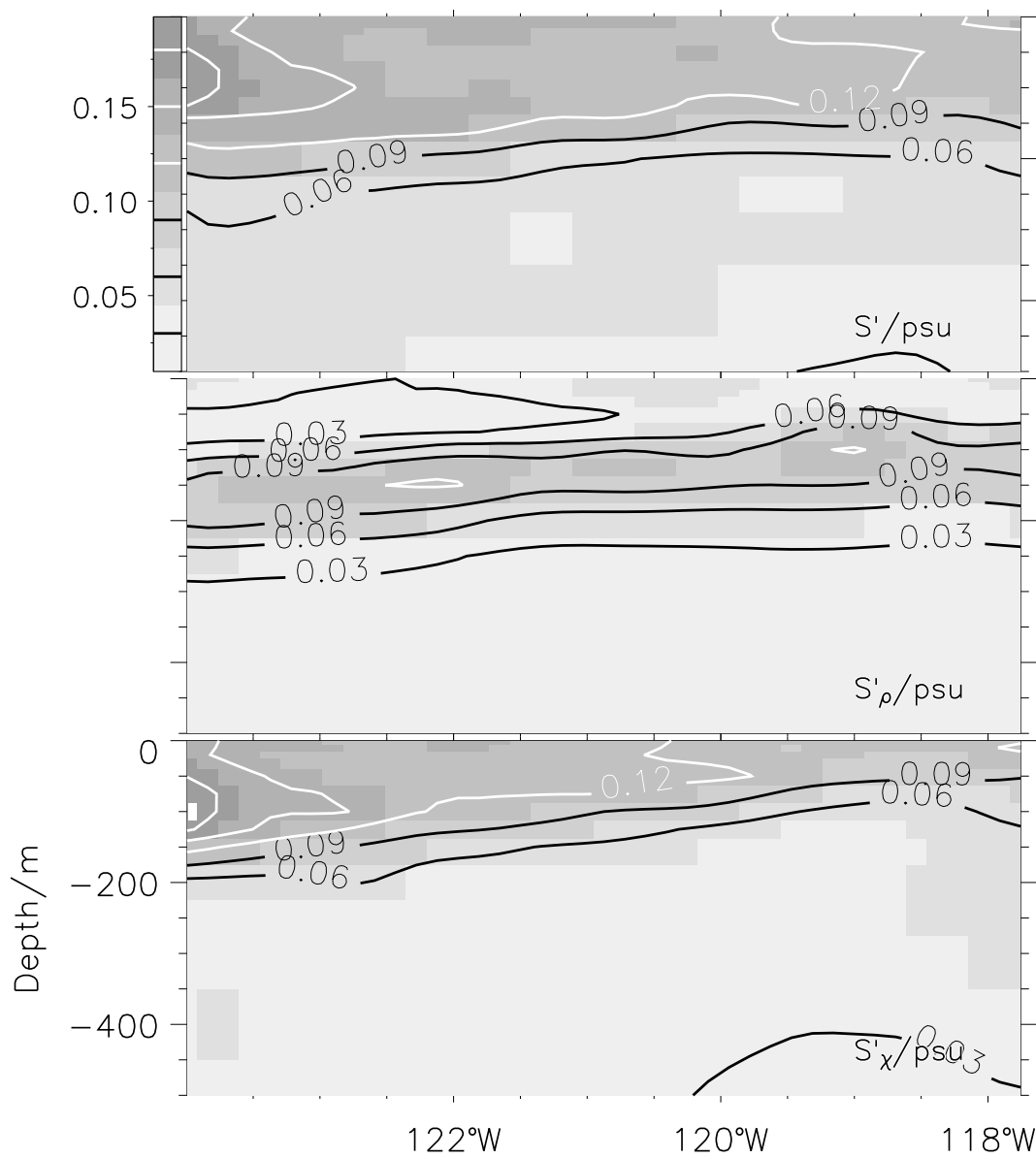


**Fig. 9.** Variance of anomalies of salinity in psu. Top panel shows root-mean-square (rms) value of anomalies of salinity, the center panel shows the rms of anomalies of salinity associated with vertical displacements of isopycnals, and the lower panel shows the rms of salinity variations independent of density.

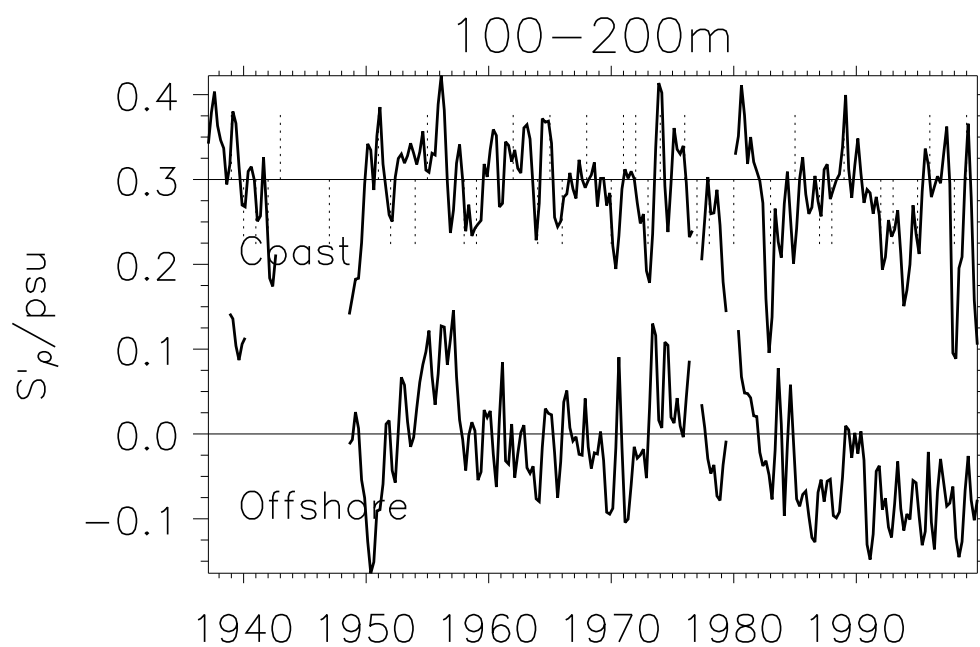


**Fig. 10.** Time series of salinity  $S'_\rho$  associated with density variations (halocline heave) in psu at depth from 100 to 200m. Top line shows variations east of  $121.5^\circ\text{W}$  ('Coast'), bottom from west of  $121.5^\circ\text{W}$  ('Offshore'). The top panel has been offset by 0.3 psu, zero anomalies are denoted by thin lines. Thin dotted lines in the upper panel denote El Niño (downward) and La Niña (upward) events.

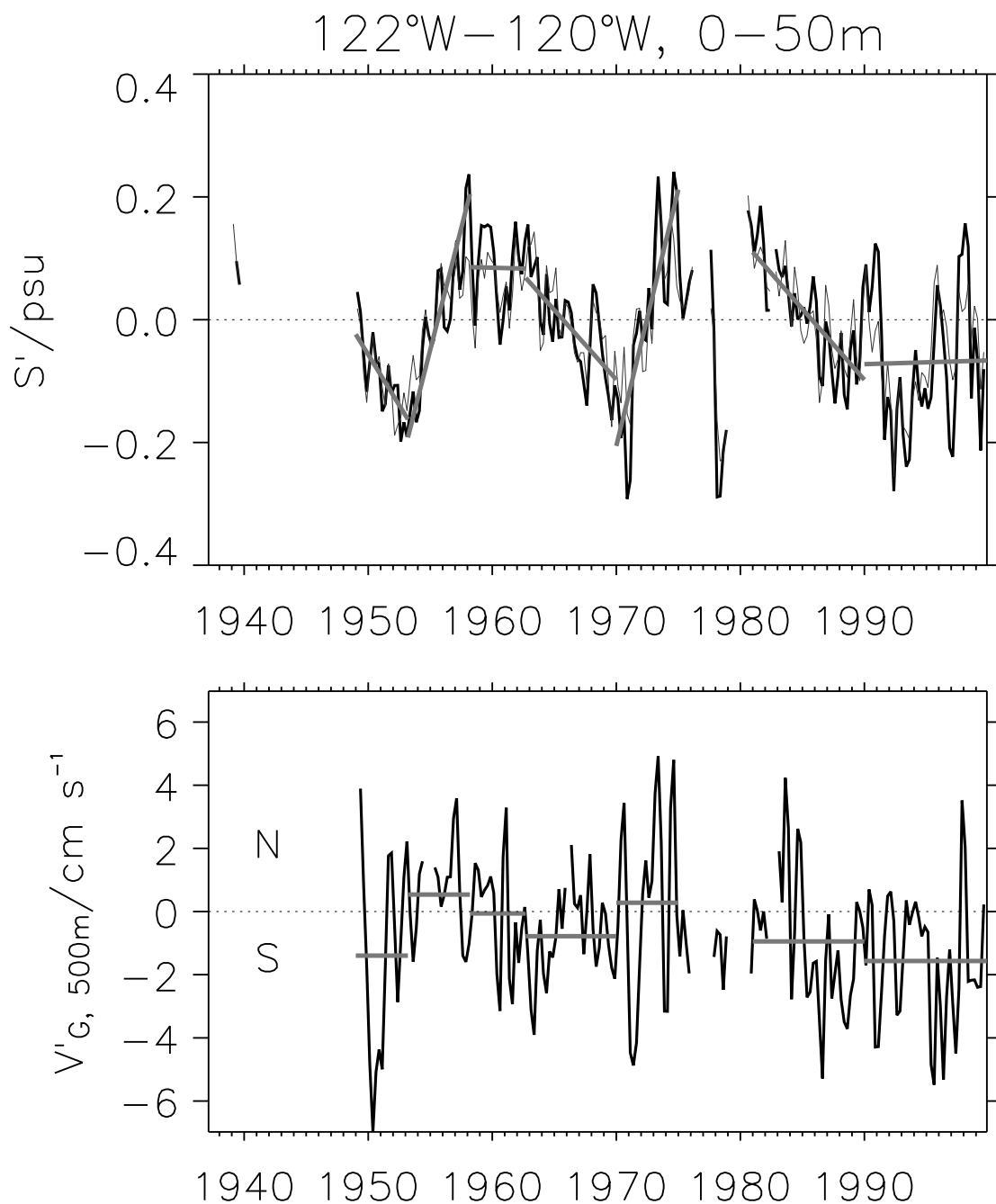


**Fig. 11.** (Top) Salinity and (bottom) along-shore geostrophic current in the salinity minimum, averaged from the surface to a depth of 50 m. Thick gray lines mark average rate of change of salinity (top) and mean geostrophic (bottom) during epochs chosen for consistent salinity trend. Positive currents correspond to poleward flows. The thin gray line (top) marks the salinity variations averaged over the top 150 m of the water column.

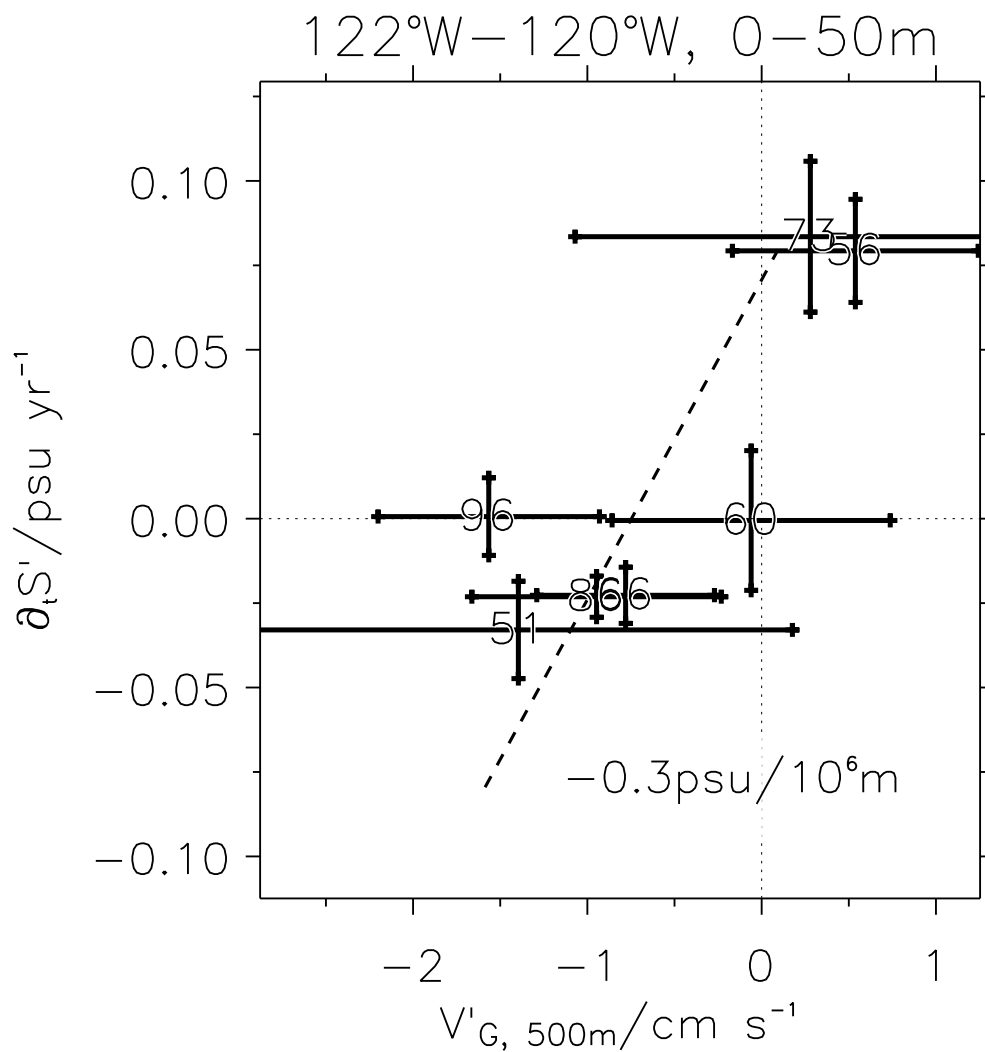


**Fig. 12.** Scatter plot of epoch averages of geostrophic velocity and rate of change of salinity. Epochs are as shown in Fig. 11 and are indicated by their center year. Error bars denote 90% confidence intervals. The climatological along-shore salinity gradient of 0.3 psu/1000 km (Fig. 1) is shown as a dashed line, and is consistent with the along-shore advection hypothesis in the 1950s, 1960s, and 1980s.

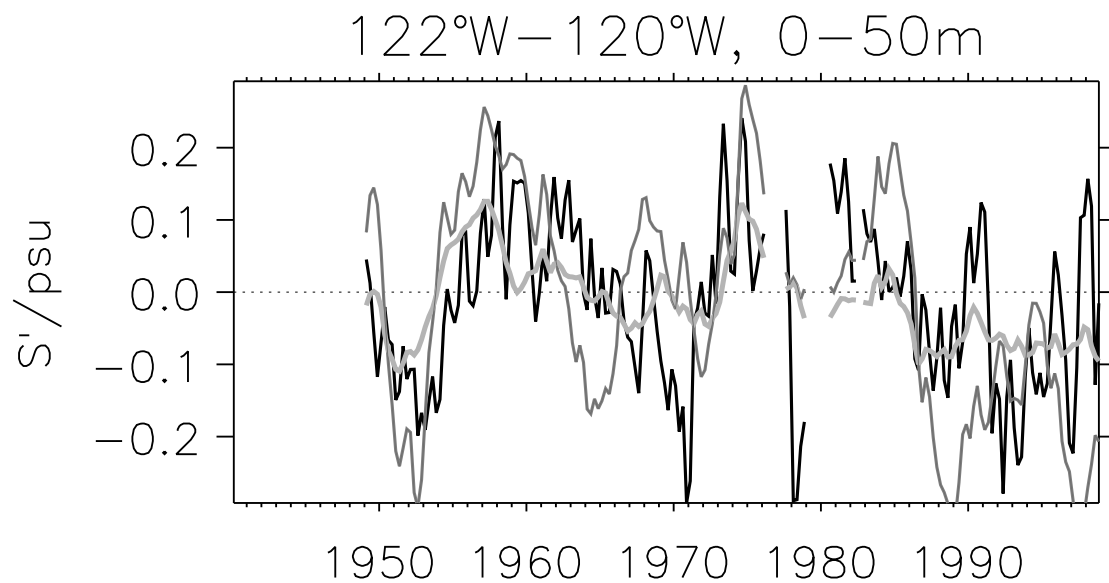


**Fig. 13.** Salinity in the salinity minimum from seasonal line 90 data (black line), expected from equation (2) forced by anomalous advection (dark gray), and least square fit of salinity variations to equation (3) forced by line-90 pressure EOFs (thick, light gray line).

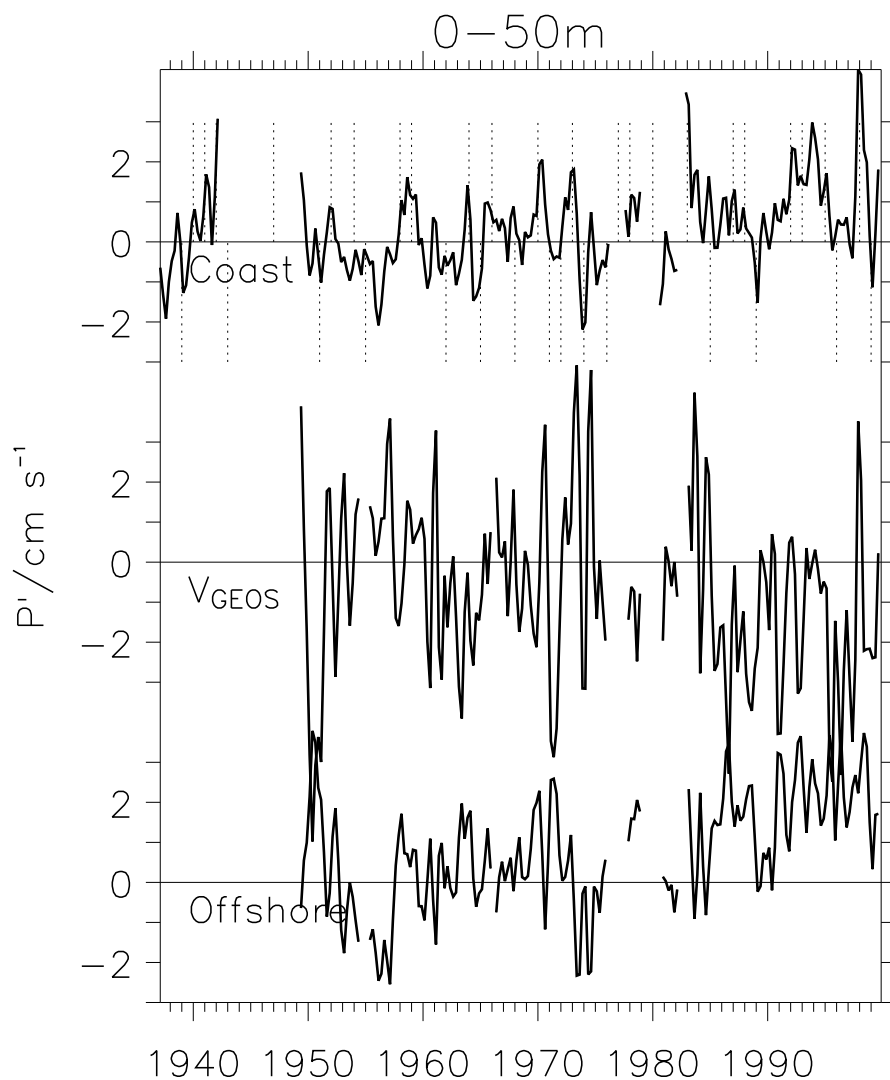


**Fig. 14.** Time series of ocean pressure relative to 500 m east (top, 'Coast') and west (bottom, 'Offshore') of  $121.2^\circ\text{W}$ , and averaged over the top 50 m of the water column. Pressure has been normalized to units of  $\text{cm s}^{-1}$  by the local Coriolis frequency, and the distance between the regions. The difference is displayed in the center panel, and is the along-shore geostrophic current, with positive numbers indicating poleward flow. The thin dotted vertical lines in the top plot denote El Niño (upward) and La Niña (downward) events.

